Carbon consequences of global hydrologic change, 1948–2009

Christopher R. Schwalm,[1] Christopher A. Williams,[1] and Kevin Schaefer[2]

Received 2 February 2011; revised 24 May 2011; accepted 20 July 2011; published 29 September 2011.

[1] Eddy covariance data (FLUXNET) provide key insights into how carbon and water fluxes covary with climate and ecosystem states. Here we merge FLUXNET data with reanalyzed evaporative fraction and dynamic land cover to create monthly global carbon flux anomalies attributable to hydrologic change from 1948 to 2009. Changes in land cover had a relative influence of <1% with an absolute effect less than uncertainty. The lack of trend globally in Net Ecosystem Productivity (NEP) attributable to hydroclimatic change masked positive trends in North America and Australia and negative trends in Africa and Asia. This spatial pattern coincided with geographic variation in hydroclimate excluding the temperature-limited high latitudes. Global NEP anomalies due to hydroclimatic variability ranged from −2.1 to +2.3 Pg C yr^{-1} relative to a global average sink of +2.8 Pg C yr^{-1}. Trends in hydroclimate-induced NEP anomalies exceeded the background mean sink in many regions.

Citation: Schwalm, C. R., C. A. Williams, and K. Schaefer (2011), Carbon consequences of global hydrologic change, 1948–2009, *J. Geophys. Res.*, *116*, G03042, doi:10.1029/2011JG001674.

1. Introduction

[2] The cycling of water in the Earth system is directly linked to global environmental change. The Clausius-Clapyeron equation posits a 7% change in specific humidity per 1°C of warming [*Huntington*, 2006] leading directly to an acceleration of the hydrological cycle. Evidence from observations [*Folland et al.*, 2001; *Allan and Soden*, 2008, *Robock et al.*, 2000] and climate models [*Allen and Ingram*, 2002; *John et al.*, 2009; *Trenberth et al.* 2003] also implicate the large-scale warming associated with greenhouse gas emissions as a driver of hydrologic change. This enhanced throughput alters the frequency, amount, and intensity of precipitation [*Trenberth et al.*, 2003] with downstream effects including an increased incidence of extreme dryness [*Dai et al.*, 2004], broad-scale increases in soil moisture [*Robock et al.*, 2000], a regime shift in global evapotranspiration [*Jung et al.*, 2010], and relatively wet areas becoming wetter while drier regions become drier [*John et al.*, 2009].

[3] Diagnosing changes in hydrologic fields and their effects on the Earth system is confounded by an uneven spatiotemporal coverage of high-quality hydrologic data [*Huntington*, 2006], shrinking observational networks [*Bates et al.*, 2008], and relatively short time series [e.g., *Wentz et al.*, 2007]. Natural variability [*Ziegler et al.*, 2003], interactions with atmospheric circulation patterns [*Arnell and Liu*, 2001], global dimming and brightening [*Wild et al.*, 2008], and regionally contrasting changes in precipitation [*Zhang et al.*, 2007] also act to complicate relationships between hydroclimate and terrestrial carbon sink strength.

[4] Understanding the interplay between hydrologic change and carbon cycling is a frontier challenge in the context of global environmental change. Because of the tight coupling of water and carbon cycling, changes in hydrologic variables influence terrestrial carbon sink strength [*Nemani et al.*, 2002; *Schwalm et al.*, 2010; *Zhao and Running*, 2010]. Here we present a bottom-up approach that extends observed footprint-scale relationships between carbon cycling and hydrologic change to global monthly maps of carbon flux anomalies from 1948 to 2009. We merge data from a global network of eddy covariance flux towers [*Baldocchi*, 2008], reanalyzed climate data [*Kalnay et al.*, 1996], and time-varying land cover [*Chini et al.*, 2009] to derive global, observationally based estimates of carbon flux attributable to hydrologic change. We address the following questions: How large are carbon sources/sinks resulting from long-term trends in hydroclimate? Which regions of the globe exhibit the largest trends? Where is the uncertainty the largest?

2. Data and Methods

2.1. Deriving Carbon Flux Anomalies

[5] We quantified the effect of hydroclimatic variability on global Net Ecosystem Productivity (NEP) using site-specific sensitivities observed at FLUXNET eddy covariance sites [*Baldocchi*, 2008], a global monitoring network of in situ CO_2 exchange between land and atmosphere. As described in detail by *Schwalm et al.* [2010], the sensitivities were calculated using empirical relationships between NEP and evaporative fraction (EF; calculated as the ratio of total latent heat to available energy). Prior to estimation both fields were aggregated to monthly values across all half-hours, day and nighttime, in a given month where greater

[1]Graduate School of Geography, Clark University, Worcester, Massachusetts, USA.
[2]National Snow and Ice Data Center, University of Colorado at Boulder, Boulder, Colorado, USA.

0148-0227/11/2011JG001674

than 90% of the half-hourly values were direct measurements or gap-filled with high confidence. These monthly values were deseasonalized and transformed into relative anomalies or z-scores, i.e., normalized to have mean zero and unit standard deviation (σ) by site and climatic season. We defined climatic season by calendar month and hemisphere, e.g., climatic winter was December, January, and February in the Northern Hemisphere and June, July, and August in the Southern Hemisphere.

[6] We then grouped the normalized data by International Geosphere-Biosphere Programme (IGBP [*Loveland et al.*, 2000]) land cover class and climatic season. Using all months within each group we regressed normalized NEP on normalized EF. The linearity of these relationships was confirmed using the Akaike information criterion. The sensitivity, i.e., the slope of the regression line, was then transformed to units g C m^{-2} mon^{-1} σ^{-1} using the biome-specific pooled standard deviation of NEP. Uncertainties for each sensitivity (see section 2.2) were calculated by combining, in quadrature, slope uncertainty from standard regression techniques and bootstrapped uncertainty of the biome-specific pooled standard deviation. Overall the sensitivities were derived using 5173 site-months from 1991 to 2006 collected at 238 sites distributed globally on an irregular grid with the highest geographical concentration in Europe and North America [*Schwalm et al.*, 2010].

[7] We used these FLUXNET-derived NEP sensitivities to generate time- and space-varying global fields of monthly NEP flux anomalies attributable to hydrologic change from 1948 to 2009 (hereafter δ_{NEP}). For scaling in space we first generated annual time series of the IGBP land cover scheme for each terrestrial pixel using (1) data from the Land Use Harmonization project (LUH [*Chini et al.*, 2009]), a harmonized set of six land cover classes for the Fifth Assessment Report of the Intergovernmental Panel on Climate Change, and (2) dynamic plant functional type (16 classes) output from the Community Land Model (CLM [*Lawrence and Chase*, 2010]). In both cases, we translated base land cover to the IGBP template. Sensitivities for each terrestrial grid cell were the weighted average of all sensitivities with weights equal to the fractional coverage of each land cover class.

[8] Dynamic climate was incorporated by linking the spatially scaled sensitivities to time-varying reanalyzed EF. To reconstruct δ_{NEP} over the longest time span possible we used National Centers for Environmental Prediction/National Center for Atmospheric Research (NCEP/NCAR) Reanalysis data [*Kalnay et al.*, 1996] from 1948 to 2009. As with the FLUXNET-derived NEP sensitivities, EF was calculated as the ratio of latent heat to available energy. Combining the time-varying maps of spatially scaled sensitivities and reanalyzed EF allowed for δ_{NEP} to be calculated for any point in time and space:

$$\delta_{NEP} = z_{EF}\left[\sum_{i=1}^{18} w_i \Delta_i\right], \quad (1)$$

where, for a given pixel and month, δ_{NEP} (g C m^{-2} $month^{-1}$) is the anomaly in NEP attributable to hydrologic change, z_{EF} is the relative anomaly of monthly EF, w_i is the fractional coverage of the 18 IGBP land cover classes, and Δ_i is the NEP sensitivity (g C m^{-2} mon^{-1} σ^{-1}) for each IGBP land cover class.

[9] In addition to δ_{NEP}, we also calculated δ_{GPP} and δ_R, the effects of hydrologic change on gross primary productivity (GPP) and R (ecosystem respiration), and their uncertainties, respectively. GPP and R were estimated using FLUXNET flux partitioning algorithms [*Reichstein et al.*, 2005] and sensitivities derived following *Schwalm et al.* [2010]. Because our approach generated anomalies attributable to hydrologic change, we used gridded NEP from CarbonTracker [*Peters et al.*, 2007] to estimate mean NEP and related this to δ_{NEP}. We also used independent monthly hydrologic fields to characterize broad-scale changes in the global water cycle: UDel precipitation from 1948 to 2008 [*Legates and Willmott*, 1990], CRU TS 3.0 precipitation from 1948 to 2006 [*Mitchell and Jones*, 2005], UDel soil moisture (midmonthly mm assuming a soil column of 150 cm depth) from 1948 to 2008 [*Willmott et al.*, 1985], and Palmer Drought Severity Index (PDSI) from 1948 to 2005 [*Dai et al.*, 2004]. Prior to analysis, all data products were regridded to a 1° latitude/longitude resolution. To be consistent with our calculated flux anomalies, we removed each grid cell's mean monthly cycle across the full record, except for PDSI, which was already in anomaly form.

[10] To separate the effects of land cover and climate, we performed three upscaling scenarios: DLDC, the baseline, used both dynamic land cover and dynamic climate. CLDC used constant land cover and dynamic climate. DLCC used dynamic land cover and constant climate. For constant climate, the middle year of the time record (1979) was repeated for the 62-year record. Constant land cover used the baseline IGBP land cover map [*Loveland et al.*, 2000]. We quantified absolute effects through differencing (effect of land cover = DLDC − CLDC; effect of climate = DLDC − DLCC) and relative influence using variance decomposition [*Schaefer et al.*, 2002].

2.2. Uncertainty Analysis

[11] Our uncertainty analysis included both uncertainty in the δ_{NEP} time series and methodological uncertainty. The latter was based on trend uncertainty in EF as well as representation error of both the underlying sensitivities and the FLUXNET network. We also calculated the overall relative confidence of our bottom-up approach by combining all methodological uncertainties.

[12] Uncertainty, one standard deviation about the mean (1σ), for the δ_{NEP} time series was estimated by combining uncertainty in land cover, NEP sensitivity, and reanalyzed EF. We calculated EF uncertainty using multiple overlapping retrospective analyses from the Multimodel Analysis for the Coordinated Enhanced Observing Period (CEOP [*Bosilovich et al.*, 2009]) data set, an ensemble of 10 global reanalysis monthly products from October 2002 to December 2004 that included the NCEP/NCAR Reanalysis. EF uncertainty was estimated as 1σ across all ensemble members for each terrestrial pixel. We averaged these values to a mean cycle of uncertainty for the full analysis period. For the FLUXNET-based sensitivities we used the uncertainty associated with observed linear relationships between NEP and EF from standard regression techniques combined with the bootstrapped

standard deviation of NEP [*Schwalm et al.*, 2010]. These sources of uncertainty were combined for each grid cell by the use of Monte Carlo methods, and also across grid cells in quadrature to global yearly values. For land cover we estimated global yearly values of δ_{NEP} using translated IGBP classes from LUH, the baseline, and CLM with time-varying reanalyzed EF. As a robust estimate of uncertainty, we calculated their mean absolute deviation for the 62-year period and scaled this by 1.4826 [*Jung et al.*, 2009] to obtain 1σ.

[13] To quantify the uncertainty of long-term EF dynamics, we calculated the coefficient of variation in EF trend using four reanalysis products. For the global changes in EF from 1948 to 2009, we effectively assumed that the NCEP/NCAR reanalysis was an unbiased forcing data set, even while recognizing limitations noted by others concerning, e.g., downwelling shortwave [*Sheffield et al.*, 2006], relative humidity [*Dessler and Davis*, 2010], and soil moisture [*Lu et al.*, 2005]. In addition to NCEP/NCAR, we estimated trends in EF from 1979 to 2008 using the NCEP/Department of Energy (DOE) [*Kanamitsu et al.*, 2002], MERRA [*Bosilovich et al.*, 2008], and National Oceanic and Atmospheric Administration-Cooperative Institute for Research in Environmental Sciences (NOAA-CIRES) [*Compo et al.*, 2011] reanalyses. The time window was determined by the longest span covered by all four products. We calculated a map of the coefficient of variation in EF trend (*CV*) as the mean trend divided by its standard deviation using all four reanalyses at each pixel. While this ignored potential effects of switching from the nonsatellite to the satellite era [e.g., *Dessler and Davis*, 2010], it offered a 30-year window to evaluate the robustness of the NCEP/NCAR EF trends.

[14] Representation error involved two distinct characterizations of uncertainty that were subsequently combined with uncertainty in EF trend to assess relative confidence. The first characterization addressed statistical reliability of NEP sensitivity to EF. For this we generated a signal-to-noise ratio (SNR) map where each grid cell was populated by the ratio of its gridded sensitivity (cf. equation 1) normalized by its uncertainty. SNR values in excess of two represented sensitivities distinct from zero with at least 95% confidence. The second characterization of uncertainty addressed the network representativeness of FLUXNET. We tabulated the number of sites used for sensitivity derivation in all intersections of climate type (Köppen-Geiger group and type classes [*Peel et al.*, 2007]) and biome (IGBP land cover class [*Loveland et al.*, 2000]). We then mapped this globally based on each pixel's climate by biome setting to obtain a map quantifying the network's degree of representation.

[15] Last, we created a map of relative confidence for the upscaled fluxes by combining the uncertainty in EF trend, the signal-to-noise ratio of NEP sensitivity, and FLUXNET representativeness. This allowed for a nonparametric ranking of the degree of extrapolation and overall robustness [cf. *Jung et al.*, 2009] of the hydroclimatically driven NEP trends derived in this work. Prior to combination all three maps were transformed to ranks and then binned by decile. The three binned maps were then combined additively and mapped to four ordinal classes of relative confidence: A value of 0 indicated the lowest relative confidence (more uncertainty/less representativeness). A value of 3 indicated the highest relative confidence (less uncertainty/more representativeness).

3. Results and Discussion

[16] The global time series did not exhibit a long-term trend in δ_{NEP}, δ_{GPP}, or δ_R (Figure 1). During the 62-year record, the global annual δ_{NEP} showed considerable variability, ranging from −2.1 to +2.3 Pg C yr^{-1} relative to an average 2000 to 2006 sink of +2.8 Pg C yr^{-1} [*Canadell et al.*, 2007]. δ_{GPP} was typically greater than δ_R, mimicking patterns observed on footprint to biome scales [*Schwalm et al.*, 2010]. The gross fluxes, δ_{GPP} and δ_R, were largely in phase and ~50% larger than δ_{NEP}, i.e., their degree of compensation resulted in a more conservative δ_{NEP} trajectory. Total uncertainty was an order of magnitude less than the observed range over the 62-year record and was driven by uncertainty in land cover. Uncertainty in δ_{GPP} was greatest, followed by δ_R and δ_{NEP} (0.69, 0.49, and 0.36, Pg C yr^{-1}, respectively). Despite the large uncertainty associated with land cover, time series of all carbon fluxes based on LUH and CLM were highly correlated ($r \geq 0.92$; $p < 10^{-6}$), such that hereafter we only consider LUH.

[17] Continental scale trends were statistically significant and canceled each other, resulting in a zero global trend (Table 1). North America showed a large positive trend, while Asia and Africa show negative trends. Like the global time series, continental trends in δ_{GPP} were greater than trends in δ_R. Note that the trends in δ_{GPP} and δ_R were significant for North America, while the trend in δ_{NEP} was not and the opposite was true for Asia.

[18] Temporal variability at all spatial scales was driven by hydrologic change as opposed to changes in land cover. The mean absolute deviation between DLDC and CLDC scenarios, the effect of land cover, was 0.029 Pg C yr^{-1} globally; two orders of magnitude less than the observed range in δ_{NEP} and less than uncertainty. DLDC and CLDC were also highly correlated ($r = 0.998$; $p < 10^{-6}$). Furthermore, relative influence was 99.8% for climate and 0.2% for land cover. This dominance of climate was present (>99.5% relative influence) across all continents and all carbon fluxes.

[19] Despite the dominance of climate there was a significant linear trend (= −0.001 Pg C yr^{-1}; $p < 10^{-6}$) in δ_{NEP} associated with land cover; indicating the changes in global land cover from 1948 to 2009 were conducive to decreased uptake of CO_2 conditioned on hydrologic change. This trend's effect and the effect of land cover in general were negligible in magnitude. However, transient effects, e.g., flushes of respiration due to land clearing [*Amiro et al.*, 2010], were not estimated, since we assumed that steady state as one land cover type was replaced by another. Such transient effects influence the background mean NEP, whereas our results indicated that changes in carbon flux attributable to hydrologic change were driven by climate.

[20] Geographic variation in T_{NEP}, the trend in δ_{NEP} over the 62-year period, yielded well-defined regions of enhanced uptake and outgassing of CO_2 (Figure 2a). Prominent zones of enhanced CO_2 uptake were located in the conterminous United States, south central Canada, southern Brazil, and southern Africa. Enhanced outgassing dominated the Sahel region of Africa, Europe, and large parts of China. The largest region lacking any significant long-term trend was

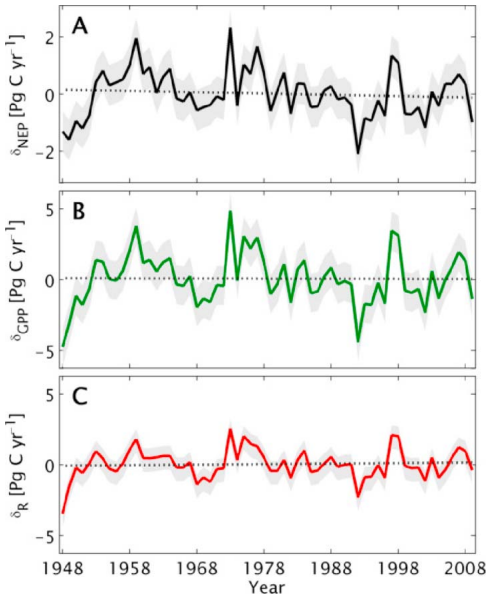

Figure 1. Time series of carbon flux attributable to hydrologic change from 1948 to 2009. Flux is either (a) δ_{NEP}, (b) δ_R, or (c) δ_{GPP}. Dashed line shows zero reference line. Trends lines are not significant ($p > 0.44$) and are visually indistinguishable from the zero reference line. Gray envelope is 95% interval ($\pm 2\sigma$) that combines uncertainties in EF, sensitivity, and land cover in quadrature. Note change in y-axis scale.

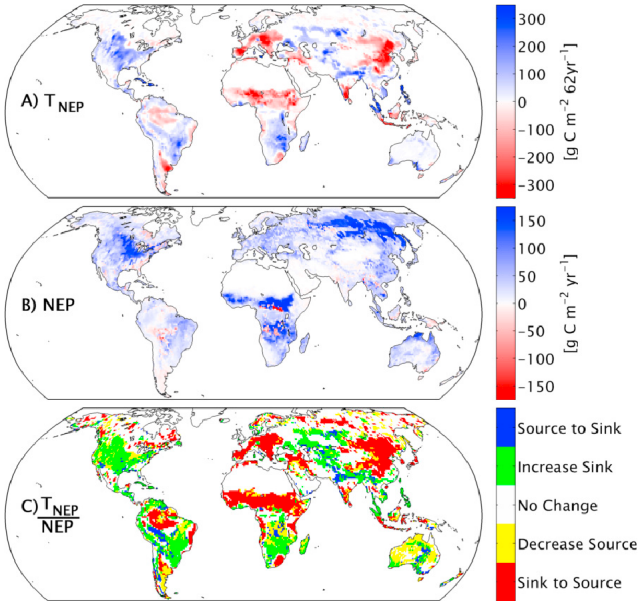

Figure 2. Long-term trend and mean NEP. (a) 62-year trend (T_{NEP}) in NEP attributable to hydrologic change. (b) CarbonTracker mean NEP from 2001 to 2008. (c) Regions where T_{NEP} induced a change from a source to sink (blue), a sink to source (red), an increase sink in CO_2 uptake (green), or a decrease source in CO_2 uptake (yellow). Nonvegetated grid cells and those without significant trend or change shown in white.

the northern high latitudes. However, temperature dominates interannual variability in NEP in this region [*Nemani et al.*, 2003; *Schaefer et al.*, 2002; *Yi et al.*, 2010], and no significant influence of changing hydroclimate on carbon flux was expected.

[21] T_{NEP} was large compared with long-term NEP averages from CarbonTracker [*Peters et al.*, 2007] (Figure 2b). Roughly 25% by area of the vegetated terrestrial biosphere had a magnitude of T_{NEP} greater than background mean NEP. This included significant areas (Figure 2c) where T_{NEP} acted to switch a source to a sink (~4%) or sink to a source (20%), in agreement with the secular trend of increased dryness [*Dai et al.*, 2004] and downstream effects on CO_2 uptake [*Schwalm et al.*, 2010]. CarbonTracker only covers 2001 to 2008 and is likely biased high relative to the true 1948–2008 mean NEP. Global NEP from 1949 to 2008 has shown an upward trend [*Le Quéré et al.*, 2009], indicating that the effects of long-term change in hydroclimate on NEP were likely greater than we estimate.

[22] Trends in δ_{NEP} were strong enough to change many regions from a sink to a source (Figure 2c). The tropics, eastern China, and Europe exhibited spatially coherent transitions from a sink to a source. Over vast tracts of the Western Hemisphere, hydroclimatic variability acted to increase CO_2 uptake; including regions with sources becoming smaller in magnitude. These features were not linked to land cover class, change in land cover, or background NEP ($|r| < 0.05$; $p > 0.15$), but rather to the underlying trends in hydrologic fields (Figure 3).

[23] To understand the spatial clustering in T_{NEP} we first focus on North America and Europe. This emphasis is based on the high density of FLUXNET sites in both regions [*Baldocchi*, 2008] to maximize the robustness of the bottom-up approach applied here. In general, the trend in EF and hence δ_{NEP} matched the sign of long-term changes in hydrologic variables such as precipitation and PDSI (Figure 3). Whereas Europe became drier (negative trends in soil moisture and PDSI), the conterminous United States became wetter (positive trends in precipitation, soil moisture, and PDSI). A modeling exercise has similarly indicated that enhanced wetness has modulated the strength of the midlatitude terrestrial sink across North America [*Nemani et al.*, 2002].

[24] Outside North America and Europe, other regions exhibited inverse trends. For example, in the Ural and Volga regions of Russia and Kazakhstan (Figure 3), this was linked to seasonality and dominant vegetation type. Grasslands, the dominant land cover class in this region, exhibited a clear

Table 1. Trend in Carbon Flux Attributable to Hydrologic Change from 1948 to 2009[a]

Region	Trend (Pg C yr^{-1})		
	δ_{NEP}	δ_{GPP}	δ_R
Global	−0.005	−0.001	0.004
North America	**0.011**	**0.025**	**0.013**
South America	0.003	**0.015**	**0.012**
Europe	−0.005	−0.008	−0.002
Asia	**−0.008**	−0.011	−0.003
Africa	**−0.008**	**−0.029**	**−0.022**
Australia[b]	**0.003**	**0.014**	**0.011**

[a]Bold values significant at $\alpha = 0.05$.
[b]Australia includes tropical Southeast Asia.

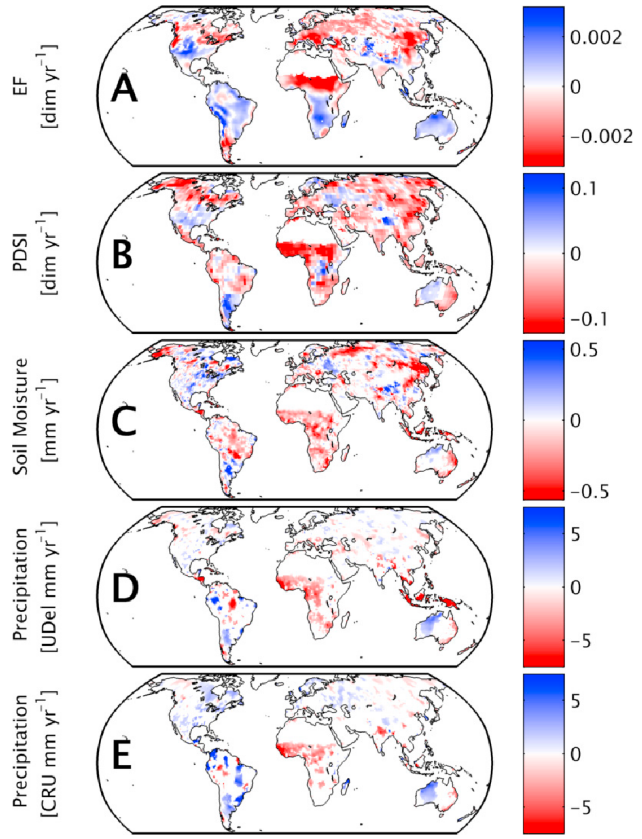

Figure 3. Trends in hydroclimatic fields. (a) Evaporative fraction (EF) anomaly from NCEP/NCAR Reanalysis [*Kalnay et al.*, 1996] from 1948 to 2009. (b) Palmer Drought Severity Index (PDSI) [*Dai et al.*, 2004] from 1948 to 2005. (c) UDel soil moisture anomaly (v1.03) [*Willmott et al.*, 1985] from 1948 to 2008. (d) UDel precipitation anomaly (v2.1) [*Legates and Willmott*, 1990] from 1948 to 2008. Panel E: CRU precipitation anomaly (TS 3.0) [*Mitchell and Jones*, 2005] from 1948 to 2006. Only significant ($p \leq 0.05$) values shown; based on linear trends derived using deseasonalized monthly values scaled to 1 year. Nonvegetated grid cells shown in white. Red values indicate increasing dryness.

seasonality in response to changes in hydroclimate [*Schwalm et al.*, 2010] with zero sensitivity in climatic fall or winter. These inverse trends (declining EF but increasing δ_{NEP}) indicated that changes in the water cycle were skewed toward climatic seasons with zero sensitivity, i.e., negative EF trends during climatic fall and winter were larger than positive ones in climatic spring and summer.

[25] For the tropics of South America and Africa, the dominant land cover class is evergreen broadleaf forest. During the dry season, decreased wetness was found coincident with an increase in CO_2 uptake in this forested type [*Saleska et al.*, 2007; *Schwalm et al.*, 2010]. Because the tropics are radiation-limited [*Teuling et al.*, 2009], this baseline sensitivity followed from the link between drier conditions and a decrease in cloudiness with an increase in downwelling radiation and concomitant increase in carbon uptake [*Bonal et al.*, 2008; *Saleska et al.*, 2007]. Globally, the spatial patterning of agreement between T_{NEP} (Figure 2a) and trend in EF (Figure 3a) across the 62-year hindcast period was modulated by intraannual variability in both trends relative to the baseline sensitivities.

[26] While, for most regions, trends between δ_{NEP} (Figure 2a) and EF (Figure 3a), as well as across independent characterizations of the global water cycle, were in agreement, some regions exhibited discrepancies, e.g., the Congo Basin of Africa. This was related to sparse sampling networks in several regions [*Bates et al.*, 2008; *Huntington*, 2006] and what each metric represents. The global water cycle metrics reference demand and supply in varying degrees. EF and PDSI take both demand and supply of plant available water into account, whereas soil moisture and precipitation focus solely on supply. PDSI also includes explicit temperature dependence.

[27] A further caveat concerns the uncertainty in the independent characterizations of the global water cycle (Figure 3). For precipitation, a key boundary condition for

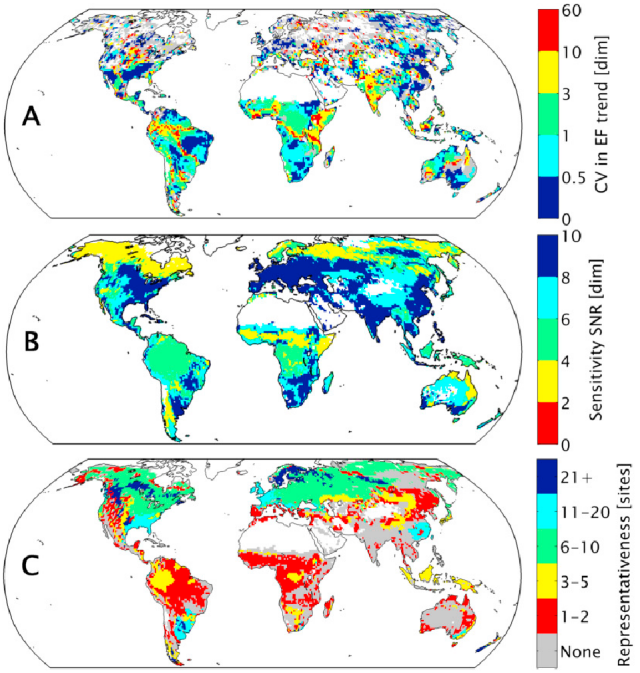

Figure 4. Uncertainty in EF trend, NEP sensitivities, and representativeness of FLUXNET. (a) Coefficient of variation (*CV*) for trend in EF. Map shows ratio of standard deviation in EF trend over mean EF trend across four reanalysis products: NCEP/NCAR [*Kalnay et al.*, 1996], NCEP/DOE [*Kanamitsu et al.*, 2002], MERRA [*Bosilovich et al.*, 2008], and NOAA-CIRES [*Compo et al.*, 2011]. Time coverage is period of longest overlap from 1979 to 2008. *CV* values of 0 (gray) occur only when a single reanalysis has a significant trend in EF. Areas without significant trend ($p > 0.05$) across all four reanalysis products shown in white. (b) Signal-to-noise ratio (SNR) of gridded NEP sensitivity. Map shows NEP sensitivity (signal) normalized by its uncertainty (1σ, noise). Values of greater than 2 indicate nonzero sensitivities with at least 95% confidence. (c) Intersection of Köppen-Geiger climate, group and type only [*Peel et al.*, 2007], with IGBP land cover class [*Loveland et al.*, 2000]. Representativeness values are from a cross-tabulation of FLUXNET sites used in sensitivity derivation mapped using table lookup. In Figures 4a–4c, nonvegetated areas shown in white.

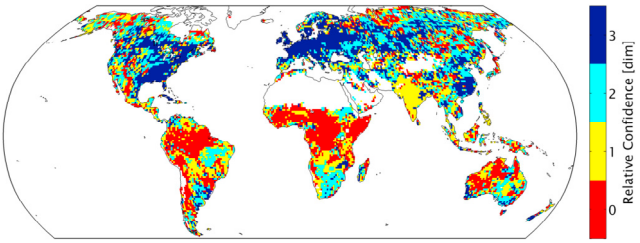

Figure 5. Relative confidence in estimated flux anomalies based on the combination of uncertainty in EF trend, signal-to-noise ratio of NEP sensitivity, and representativeness of FLUXNET. A value of 0 indicates low confidence and value of 3 indicates high confidence. Nonvegetated areas are shown in white.

the hydrologic cycle, spatial means, spatial percentiles, and trends globally exhibit high degrees of similarity across observation-based products [*Fekete et al.*, 2004; *Nickl et al.*, 2010]. However, less similarity is seen in global averages across reanalysis products [*Bosilovich et al.*, 2008]. Furthermore, the geography of precipitation may show pronounced regional dissimilarities [*Fekete et al.*, 2004; *Yang et al.*, 2005]. In this study the precipitation trends derived using the UDel (Figure 3d) and CRU (Figure 3e) products showed broad-scale agreement, e.g., Africa and Australia (Figure 3d and 3e), but also regional differences, e.g., the upper Amazon basin. Despite these limitations, the overall consistency and agreement between broad-scale trends in independent hydrologic variables and EF (Figure 3a) lend confidence to our reported patterns of T_{NEP} (Figure 2a).

[28] The coefficient of variation for the trend in EF (*CV*; Figure 4a) showed that overall NCEP/NCAR EF was generally representative of trends in the global water cycle. *CV* exhibited a large positive skew (mean = 9.52 and maximum = ~25,000) with a median value of 0.43. The regions with the highest degree of uncertainty were the tropics and the Indian subcontinent. In the Pampas region of Argentina, the uncertainty in EF (Figure 4a) was corroborated by the positive trends documented in four independent realizations of the global water cycle, PDSI, soil moisture, and two precipitation products (Figure 3), versus the negative trend in NCEP/NCAR EF.

[29] Gridded sensitivities exhibited a pattern similar to uncertainty in EF trend (Figure 4b). When expressed as a SNR we found values above two across the full vegetated biosphere, lending confidence to our overall approach. Areas with smaller SNRs occurred in the tropics, the Sahel region of Africa, and the temperature-limited northern high latitudes. For regions dominated by open shrublands, savannahs, and/or wetlands, the signal-to-noise ratios were likely overestimated, because they were undersampled by FLUXNET. Only 162, 54, and 110 site months, respectively, were available for these three classes [*Schwalm et al.*, 2010]. This resulted in larger variability relative to sample size and NEP sensitivities indistinguishable from zero at 95% confidence. In open shrublands, for example, climatic summer sensitivities for both gross fluxes were ~30 g C m^{-2} mon^{-1}. However, these values effectively canceled and resulted in a net NEP sensitivity of zero.

[30] Poor sampling of these cover types, especially open shrublands, also appeared in our depiction of FLUXNET representativeness (Figure 4c). Globally, the degree of representativeness was highest for the midlatitudes of the Northern Hemisphere. Areas of marginal productivity (e.g., the steppes of Central Asia and dryland ecosystems of Australia), the Southern Hemisphere, and the tropics were sampled by relatively few towers. For open shrublands, this is especially problematic. Open shrublands exist across large gradients in climate and floristics that were not well captured with FLUXNET. This resulted in a muted NEP response on the biome level that likely masked within-biome variability. Because open shrublands occupy ~25% of the vegetated biosphere, our estimates of changes in source/sink status over the 62-year reconstruction period were likely biased downward; any positive sensitivity would exacerbate reported trends (Figure 2a).

[31] As expected, relative confidence was highest where FLUXNET towers and long-term meteorological stations showed the highest density: in the eastern conterminous United States and Europe (Figure 5). Conversely, relative confidence in our NEP trends was lowest for areas where open shrublands are dominant, the tropics and the Southern Hemisphere. Previous attempts to quantify the representativeness of FLUXNET have shown similar results. For example, *Sundareshwar et al.* [2007] used multivariate clustering of edaphic, topographic, and climatic fields, and found high levels of representativeness coincident with the higher density of FLUXNET towers and lower levels in the Indian Subcontinent, the tropics (primarily Africa and Indonesia) as well as open shrublands and dryland ecosystems globally. *Jung et al.* [2009] used model-tree ensembles and found that FLUXNET least well represented the tropics and Indian Subcontinent. Combining these literature-based assessments of representativeness with the composite uncertainty developed here underscores the need for more observations of the coupled carbon and water cycle dynamics in the tropics, open shrubland, and dryland systems globally, as well as in Southeast Asia, including India.

4. Conclusions

[32] Terrestrial landscapes have the potential to undergo large-magnitude trends in carbon uptake or release associated with long-term trends in hydrologic variables, particularly with respect to regional sources and sinks that often greatly exceed flux totals. This was most evident in China, Europe, and the Sahel region of Africa. Continued and future hydrologic trends and variability can be expected to modulate the long-term background biotic sinks for CO_2. Although the magnitude of these changes is uncertain, results presented here confirm that, even at the global scale, hydroclimatic variation can induce sizable interannual variability in terrestrial CO_2 sources and sinks.

[33] **Acknowledgments.** C.R.S., C.A.W., and K.S. were supported by U.S. National Science Foundation grant ATM-0910766.

References

Allan, R. P., and B. J. Soden (2008), Atmospheric warming and the amplification of precipitation extremes, *Science*, *321*, 1481–1484, doi:10.1126/science.1160787.

Allen, M. R., and W. J. Ingram (2002), Constraints on future changes in climate and the hydrologic cycle, *Nature*, *419*, 224–232, doi:10.1038/nature01092.

Amiro, B. D., et al. (2010), Ecosystem carbon dioxide fluxes after disturbance in forests of North America, *J. Geophys. Res.*, *115*, G00K02, doi:10.1029/2010JG001390.

Arnell, N., and C. Liu (2001), Hydrology and water resources, in *Climate Change 2001: Impacts, Adaptation, and Vulnerability*, edited by J. J. McCarthy et al., pp. 191–234, Cambridge Univ. Press, Cambridge, U. K.

Baldocchi, D. (2008), Breathing of the terrestrial biosphere: Lessons learned from a global network of carbon dioxide flux measurement systems, *Aust. J. Bot.*, *56*, 1–26, doi:10.1071/BT07151.

Bates, B. C., Z. W. Kundzewicz, S. Wu, and J. P. Palutikof (Eds.) (2008), Climate change and water, technical paper, 210 pp., Intergov. Panel on Clim. Change Secr., Geneva, Switzerland.

Bonal, D., et al. (2008), The impact of severe dry season on net ecosystem exchange in the neotropical rainforest of French Guiana, *Global Change Biol.*, *14*, 1917–1933, doi:10.1111/j.1365-2486.2008.01610.x.

Bosilovich, M., J. Chen, F. R. Robertson, and R. F. Adler (2008), Evaluation of global precipitation in reanalyses, *J. Appl. Meteorol. Climatol.*, *47*, 2279–2299, doi:10.1175/2008JAMC1921.1.

Bosilovich, M., D. Mocko, J. O. Roads, and A. Ruane (2009), A multimodal analysis for the Coordinated Enhanced Observing Period (CEOP), *J. Hydrometeorol.*, *10*, 912–934, doi:10.1175/2009JHM1090.1.

Canadell, J. G., et al. (2007), Contributions to accelerating atmospheric CO_2 growth from economic activity, carbon intensity, and efficiency of natural sinks, *Proc. Natl. Acad. Sci. U. S. A.*, *104*, 18,866–18,870, doi:10.1073/pnas.0702737104.

Chini, L. P., et al. (2009) Harmonization of global land-use scenarios for the period 1500–2100 for the 5th IPCC Assessment, *Eos Trans. AGU*, *90*(52), Fall Meet. Suppl., Abstract U11A–0002.

Compo, G. P., et al. (2011), The Twentieth Century Reanalysis Project, *Q. J. R. Meteorol. Soc.*, *137*, 1–28, doi:10.1002/qj.776.

Dai, A., K. E. Trenberth, and T. Qian (2004), A global data set of Palmer Drought Severity Index for 1870–2002: Relationship with soil moisture and effects of surface warming, *J. Hydrometeorol.*, *5*, 1117–1130, doi:10.1175/JHM-386.1.

Dessler, A. E., and S. M. Davis (2010), Trends in tropospheric humidity from reanalysis systems, *J. Geophys. Res.*, *115*, D19127, doi:10.1029/2010JD014192.

Fekete, B. M., C. J. Vorosmarty, J. O. Roads, and C. J. Willmot (2004), Uncertainties in precipitation and their impacts on runoff estimates, *J. Clim.*, *17*, 294–304, doi:10.1175/1520-0442(2004)017<0294:UIPATI>2.0.CO;2.

Folland, C. K., et al. (2001), Observed climate variability and change, in *Climate Change 2001: The Scientific Basis*, edited by J. T. Houghton et al., pp. 99–182, Cambridge Univ. Press, Cambridge, U. K.

Huntington, T. G. (2006), Evidence for intensification of the global water cycle: Review and synthesis, *J. Hydrol.*, *319*, 83–95, doi:10.1016/j.jhydrol.2005.07.003.

John, V. O., R. P. Allan, and B. J. Soden (2009), How robust are observed and simulated precipitation responses to tropical ocean warming?, *Geophys. Res. Lett.*, *36*, L14702, doi:10.1029/2009GL038276.

Jung, M., M. Reichstein, and A. Bondeau (2009), Towards global empirical upscaling of FLUXNET eddy covariance observations: Validation of a model tree ensemble approach using a biosphere model, *Biogeosciences*, *6*, 2001–2013, doi:10.5194/bg-6-2001-2009.

Jung, M., et al. (2010), A recent decline in the global land evapotranspiration trend due to limited moisture supply, *Nature*, *467*, 951–954, doi:10.1038/nature09396.

Kalnay, E., et al. (1996), The NCEP/NCAR 40-Year Reanalysis Project, *Bull. Am. Meteorol. Soc.*, *77*, 437–471, doi:10.1175/1520-0477(1996)077<0437:TNYRP>2.0.CO;2.

Kanamitsu, M., W. Ebisuzaki, J. Woollen, S.-K. Yang, J. Hnilo, M. Fiorino, and G. L. Potter (2002), NCEP-DOE AMIP-II reanalysis (R-2), *Bull. Am. Meteorol. Soc.*, *83*, 1631–1643.

Lawrence, P. J., and T. N. Chase (2010), Investigating the climate impacts of global land cover change in the community climate system model, *Int. J. Climatol.*, *30*, 2066–2087, doi: 10.1002/joc.2061.

Legates, D. R., and C. J. Willmott (1990), Mean seasonal and spatial variability in gauge-corrected, global precipitation, *Int. J. Climatol.*, *10*, 111–127, doi:10.1002/joc.3370100202.

Le Quéré, C., et al. (2009), Trends in the sources and sinks of carbon dioxide, *Nat. Geosci.*, *2*, 831–836, doi:10.1038/ngeo689.

Loveland, T. R., B. C. Reed, J. F. Brown, D. O. Ohlen, J. Zhu, L. Yang, and J. W. Merchant (2000), Development of a global land cover characteristics database and IGBP DISCover from 1-km AVHRR data, *Int. J. Remote Sens.*, *21*, 1303–1330, doi:10.1080/014311600210191.

Lu, C. H., M. Kanamitsu, J. O. Roads, W. Ebisuzaki, K. E. Mitchell, and D. Lohmann (2005), Evaluation of soil moisture in the NCEP-NCAR and NCEP-DOE Global Reanalyses, *J. Hydrometeorol.*, *6*, 391–408, doi:10.1175/JHM427.1.

Mitchell, T. D., and P. D. Jones (2005), An improved method of constructing a database of monthly climate observations and associated high-resolution grids, *Int. J. Climatol.*, *25*, 693–712, doi:10.1002/joc.1181.

Nemani, R., M. White, P. Thornton, K. Nishida, S. Reddy, J. Jenkins, and S. Running (2002), Recent trends in hydrological balance have enhanced the terrestrial carbon sink in the United States, *Geophys. Res. Lett.*, *29*(10), 1468, doi:10.1029/2002GL014867.

Nemani, R. R., et al. (2003), Climate driven increases in global terrestrial net primary production from 1982 to 1999, *Science*, *300*, 1560–1563, doi:10.1126/science.1082750.

Nickl, E., C. J. Willmott, K. Matsuura, and S. M. Robeson (2010), Changes in annual land-surface precipitation over the twentieth and early twenty-first century, *Ann. Assoc. Am. Geogr.*, *100*(4), 729–739, doi:10.1080/00045608.2010.500241.

Peel, M. C., B. L. Finlayson, and T. A. McMahon (2007), Updated world map of the Köppen-Geiger climate classification, *Hydrol. Earth Syst. Sci.*, *11*, 1633–1644, doi:10.5194/hess-11-1633-2007.

Peters, W., et al. (2007), An atmospheric perspective on North American carbon dioxide exchange: CarbonTracker, *Proc. Natl. Acad. Sci. U. S. A.*, *104*, 18,925–18,930, doi:10.1073/pnas.0708986104.

Reichstein, M., et al. (2005), On the separation of net ecosystem exchange into assimilation and ecosystem respiration: Review and improved algorithm, *Global Change Biol.*, *11*, 1424–1439, doi:10.1111/j.1365-2486.2005.001002.x.

Robock, A., et al. (2000), The Global Soil Moisture Data Bank, *Bull. Am. Meteorol. Soc.*, *81*, 1281–1299, doi:10.1175/1520-0477(2000)081<1281:TGSMDB>2.3.CO;2.

Saleska, S. R., K. Didan, A. R. Huete, and H. R. da Rocha (2007), Amazon forests green-up during 2005 drought, *Science*, *318*, 612, doi:10.1126/science.1146663.

Schaefer, K. S., A. S. Denning, N. Suits, J. Kaduk, I. Baker, S. Los, and L. Prihodko (2002), Effect of climate on interannual variability of terrestrial CO_2 fluxes, *Global Biogeochem. Cycles*, *16*(4), 1102, doi:10.1029/2002GB001928.

Schwalm, C. R., et al. (2010), Assimilation exceeds respiration sensitivity to drought: A FLUXNET synthesis, *Global Change Biol.*, *16*, 657–670, doi:10.1111/j.1365-2486.2009.01991.x.

Sheffield, J., G. Goteti, and E. F. Wood (2006), Development of a 50-yr, high resolution global dataset of meteorological forcings for land surface modeling, *J. Clim.*, *19*, 3088–3111, doi:10.1175/JCLI3790.1.

Sundareshwar, P. V., et al. (2007), Environmental monitoring network for India, *Science*, *316*, 204–205, doi:10.1126/science.1137417.

Teuling, A. J., et al. (2009), A regional perspective on trends in continental evaporation, *Geophys. Res. Lett.*, *36*, L02404, doi:10.1029/2008GL036584.

Trenberth, K. E., A. Dai, R. M. Rasmussen, and D. B. Parsons (2003), The changing character of precipitation, *Bull. Am. Meteorol. Soc.*, *84*, 1205–1217, doi:10.1175/BAMS-84-9-1205.

Wentz, F. J., L. Ricciardulli, K. Hilburn, and C. Mears (2007), How much more rain will global warming bring?, *Science*, *317*, 233–235, doi:10.1126/science.1140746.

Wild, M., J. Grieser, and C. Schär (2008), Combined surface solar brightening and increasing greenhouse effect support recent intensification of the global land-based hydrological cycle, *Geophys. Res. Lett.*, *35*, L17706, doi:10.1029/2008GL034842.

Willmott, C. J., C. M. Rowe, and Y. Mintz (1985), Climatology of the terrestrial seasonal water cycle, *J. Climatol.*, *5*, 589–606, doi:10.1002/joc.3370050602.

Yang, D., D. Kane, Z. Zhang, D. Legates, and B. Goodison (2005), Bias corrections of long-term (1973–2004) daily precipitation data over the northern regions, *Geophys. Res. Lett.*, *32*, L19501, doi:10.1029/2005GL024057.

Yi, C., et al. (2010), Climate control of terrestrial carbon exchange across biomes and continents, *Environ. Res. Lett.*, *5*, 034007, doi:10.1088/1748-9326/5/3/034007.

Zhang, X., et al. (2007), Detection of human influence on twentieth-century precipitation trends, *Nature*, *448*, 461–465, doi:10.1038/nature06025.

Zhao, M., and S. W. Running (2010), Drought-Induced reduction in global terrestrial net primary production from 2000 through 2009, *Science*, *329*, 940–943, doi:10.1126/science.1192666.

Ziegler, A. D., J. Sheffield, E. P. Maurer, B. Nijssen, E. F. Wood, and D. P. L. Lettenmaier (2003), Detection of intensification in global- and continental-scale hydrological cycles: Temporal scale of evaluation, *J. Clim.*, *16*, 535–547, doi:10.1175/1520-0442(2003)016<0535:DOIIGA>2.0.CO;2.

K. Schaefer, National Snow and Ice Data Center, University of Colorado at Boulder, Boulder, CO 80309, USA.

C. R. Schwalm and C. A. Williams, Graduate School of Geography, Clark University, Worcester, MA 01610, USA. (cschwalm@clarku.edu)